JACS
JOURNAL OF THE AMERICAN CHEMICAL SOCIETY
Article
pubs.acs.org/JACS

Structurally Well-Defined Sigmoidal Gold Clusters: Probing the Correlation between Metal Atom Arrangement and Chiroptical Response

Xin He,[†] Yuechao Wang,[‡] Hong Jiang,[‡] and Liang Zhao*[,†]

[†]The Key Laboratory of Bioorganic Phosphorus Chemistry & Chemical Biology (Ministry of Education), Department of Chemistry, Tsinghua University, Beijing 100084, China

[‡]Beijing National Laboratory for Molecular Sciences, State Key Laboratory of Rare Earth Materials Chemistry and Applications, Institute of Theoretical and Computational Chemistry, College of Chemistry and Molecular Engineering, Peking University, Beijing 100871, China

Supporting Information

ABSTRACT: Asymmetric arrangement of metal atoms is crucial for understanding the chirality origin of chiral metal nanoclusters and facilitating the design and development of new chiral catalysts and chiroptical devices. Here, we describe the construction of four asymmetric gold and gold−silver clusters by chirality transfer from diimido ligands. The acquired metal clusters show strong circular dichroism (CD) response with large anisotropy factors of up to 6×10^{-3}, larger than the values of most reported chiral gold nanoclusters. Regardless of the same absolute configuration of the applied three diimido ligands, sigmoidal and reverse-sigmoidal arrangements of gold atoms both can be achieved, which resultantly produce an opposite Cotton effect within a specific absorption range. On the basis of the detailed structural characterization via X-ray crystallography and contrast experiments, the chirality contribution of the imido ligand, the asymmetrically arranged metal cluster, and the chiral arrangement of aromatic rings of phosphine ligands have been qualitatively evaluated. Time-dependent DFT calculations reveal that the chiroptical property of the acquired metal clusters is mainly influenced by the asymmetrically arranged metal atoms. Correlation of asymmetric arrangements of metal atoms in clusters with their chiroptical response provides a viable means of fabricating a designable chiral surface of metal nanoclusters and opens a broader prospect for chiral cluster application.

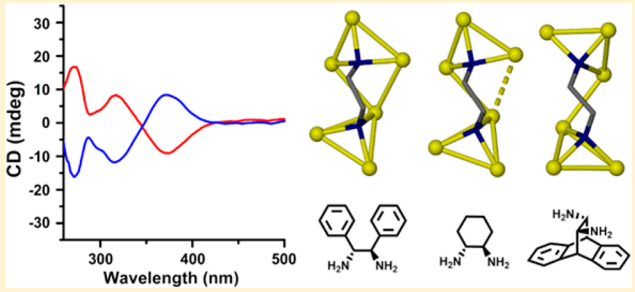

INTRODUCTION

Chirality is an intriguing feature of molecules. This fundamental geometric aspect is ubiquitous in biological systems and has a tremendous impact on the biological and pharmaceutical science through chirality-induced specificity in molecular recognition and assembly. Recent chirality studies continue to advance scientific progress in physics, chemistry, and material science, wherein chirality in nanostructures is a representative instance.[1] Chiral nano-objects,[2] especially metal nanoparticles (NPs) and nanoclusters (NCs),[3] have found many fascinating applications including enantioselective catalysis,[4] chiral recognition and separation,[5] polarization-sensitive devices,[6] and nonlinear optics,[7] etc. During the past decade, much effort has been paid to investigate the chirality in various metal NCs, not only because it is crucial in the design and development of new chiral catalysts, chiroptical devices, and for chiral nanotechnology applications, but also because it facilitates comprehension of fundamental questions on the existence and propagation of chirality at the nanoscale.[1,2]

Theoretically, chirality of metal NCs could be generated or imparted by an intrinsically chiral metallic core as well as an achiral one inside a chiral environment, which is constructed by chiral ligands, or by an asymmetric arrangement of achiral ligands or metal−ligand motifs.[3a] In this regard, both achiral and chiral ligands onto the metal NC's surface can induce the chirality generation of metal NCs. The pioneering X-ray structure determination of the gold nanocluster Au_{102}(p-MBA)$_{44}$ (p-MBA = *para*-mercaptobenzoic acid) has shown that the arrangement of the gold−sulfur staple motifs on the cluster surface forms a chiral pattern despite the use of achiral p-MBA.[8] Similar chirality generation was also reported in the gold cluster $Au_{38}(SCH_2CH_2Ph)_{24}$, wherein the chirality of the nanocluster arises from the chiral arrangement of achiral thiolates.[9] Such asymmetric arrangement of thiolate ligands around an achiral core was found to be able to provide strong Cotton effects.[10] Besides thiolates, phosphine ligands can also be applied to induce the chirality of metal NCs. An achiral polydentate phosphine ligand tris(2-(diphenylphosphino)-

Received: February 14, 2016
Published: April 12, 2016

DOI: 10.1021/jacs.6b01658
J. Am. Chem. Soc. 2016, 138, 5634−5643

ethyl)phosphine was recently employed to achieve an intrinsically chiral Au_{20} core.[11]

In contrast to a few examples of chiral metal NCs induced by achiral ligands as above, the more common methods to bestow chirality to metal NCs rely on the use of chiral ligands. Adsorption of chiral molecules not only breaks reflection symmetry of the surface and thus imparts chirality onto the metal NC, but also creates a local handedness of the surface metal atoms and consequently strengthens the asymmetry of the whole metal NC. Whetten and co-workers first demonstrated that glutathione-passivated gold nanoparticles exhibit chiroptical activity and give rise to circular dichroism (CD) responses.[12] Bürgi and co-workers further explored that the asymmetric arrangements of surface gold atoms in Au NCs could be affected by the adsorbed chiral thiolate ligands and the surface chirality can be inverted through a ligand exchange with the opposite enantiomer of the thiolate ligand.[13] These studies shed light on the pivotal role of the adsorbed chiral ligands in the chirality generation of metal NCs. More importantly, the related research has substantiated that adsorbed chiral ligands can significantly influence the chiroptical behaviors of metal NCs by distorting the arrangement of surface metal atoms or even the whole metal core. For example, Tsukuda et al. once prepared a chiral phosphine-capped $[Au_{11}(BINAP)_4X_2]^+$ (X = Cl or Br, BINAP = 2,2′-bis(diphenylphosphino)-1,1′-binaphthyl) nanocluster, and they attributed the origin of the chiroptical activity to the ligand-induced structural deformation of the Au_{11} core.[14] Garzón and co-workers' recent theoretical investigation on the geometric quantification of the chirality origins existing in intrinsic chiral clusters reported that asymmetric arrangements of surface metal atoms give a phenomenal contribution to the chirality of the whole cluster.[15] These investigations evidence the importance of asymmetric arrangements of surface metal atoms and meanwhile provide a promising avenue to achieve high chiroptical activity and strong CD response, which is critical in chiral molecular sensing.[3b,5c,16]

Despite the impressive advancement in the realm of the chirality study of metal clusters, formidable challenges still lie in (1) understanding how the chiral ligands guide the asymmetric arrangement of metal atoms at atomic level, (2) gaining insights into the origin of chirality, and (3) correlating CD response with the structural details of metal clusters. Scrutiny of available crystal structures[8,9,11,17] or theoretically predicted structures[18] of intrinsically chiral metal clusters indicates that most intrinsic chiral clusters can be divided into an achiral metal core plus one or several ligand-induced asymmetrically arranged polymetallic species at peripheral. We thus endeavor to design and synthesize a series of chiral metal clusters to clarify the role of the chiral ligands in determining the spatial arrangement of metal atoms, to provide insights into the origin of chirality, and to further probe the correlation between the metal atom arrangement and the chiroptical property.

From the topological point of view, a chiral twist in cluster shape should be easier to impress on elongated rather than spherical clusters (Figure 1a). We select three chiral 1,2-diamine ligands ($\mathbf{H_4L^1}$, $\mathbf{H_4L^2}$, and $\mathbf{H_4L^3}$ as shown in Figure 1b) as the vicinal positioning of two stereogenic centers in these ligands could enhance the chance to form an elongated chiral metal cluster. In addition, the two doubly deprotonated nitrogen atoms (RN^{2-}) would facilitate the formation of a polynuclear metal cluster due to strong electrostatic attraction. More importantly, the programmed variation of the N−C−C−N dihedral angle in these ligands can afford a regulatory factor

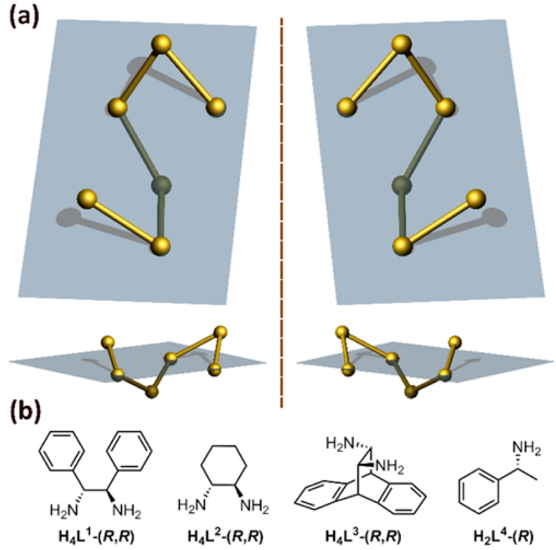

Figure 1. (a) Top and side views of sigmoidal and reverse-sigmoidal arrangements of metal atoms. (b) Molecular structures of three 1,2-diamine and a monoamine chiral ligands. Only one enantiomer of each ligand is shown.

to fine-tune the arrangement of metal atoms. A monoamine chiral ligand $\mathbf{H_2L^4}$ is utilized as a contrast example because it can be considered as one-half of $\mathbf{H_4L^1}$.

In this work, enantiopure polynuclear gold and gold−silver cluster complexes **1**−**5** were synthesized in high yields under mild conditions. They were fully characterized by X-ray crystallography and other techniques. The acquired diimido-centered gold clusters **1**−**3** (derived from the diamine ligands $\mathbf{H_4L^1}$, $\mathbf{H_4L^2}$, and $\mathbf{H_4L^3}$, respectively) and gold−silver mixed cluster **5** show strong CD response with large anisotropy factors of up to 6×10^{-3}, among the largest values reported so far for the gold clusters.[9] Continuous enlargement of the N−C−C−N torsion angles of the diamine ligands from $\mathbf{L^1}$ through $\mathbf{L^2}$ to $\mathbf{L^3}$ led to the transformation of gold atom arrangements from sigmoidal in **1** and **2** to reverse-sigmoidal in **3**. Time-dependent density functional theory (TD-DFT) calculations reveal that the intense CD responses of **1**−**3** are correlated with the asymmetrically arranged gold atoms. In contrast, the absence of the chiral cluster motif, such as the Au_3 triangle in **4** derived from the monoamine ligand $\mathbf{H_2L^4}$, caused negligible CD response. This work provides a new insight into the chirality regulation of metal clusters at atomic level and holds promise for revealing the more in-depth relationship between the chiroptical property and the asymmetric arrangement of metal atoms in chiral clusters.

RESULTS

Synthesis and Characterization of 1−5. Our synthesis was initiated with the reaction of the monoamine ligand $\mathbf{H_2L^4}$ with the gold-oxo cluster $[O(AuPPh_3)_3](BF_4)$ ($[\mathbf{Au_3O}]$)[19] according to the synthetic procedure reported by Sharp and co-workers.[20a] Upon the use of racemic $\mathbf{H_2L^4}$, colorless crystals of **4**-(*rac*) were obtained in 69% yield. Enantiopure clusters **4**-(*R*) and **4**-(*S*) as microcrystals were synthesized using the corresponding $\mathbf{H_2L^4}$-(*R*) and $\mathbf{H_2L^4}$-(*S*) as starting materials based on the same procedure. Molecular formula of **4**-(*rac*) was determined to be $[(AuPPh_3)_3(\mathbf{L^4}\text{-}(rac))](BF_4)$ by X-ray crystallography, which includes two enantiomers of $\mathbf{L^4}$ in a 1:1 ratio (Figure 2d). The imido nitrogen atom binds with

DOI: 10.1021/jacs.6b01658
J. Am. Chem. Soc. 2016, 138, 5634−5643

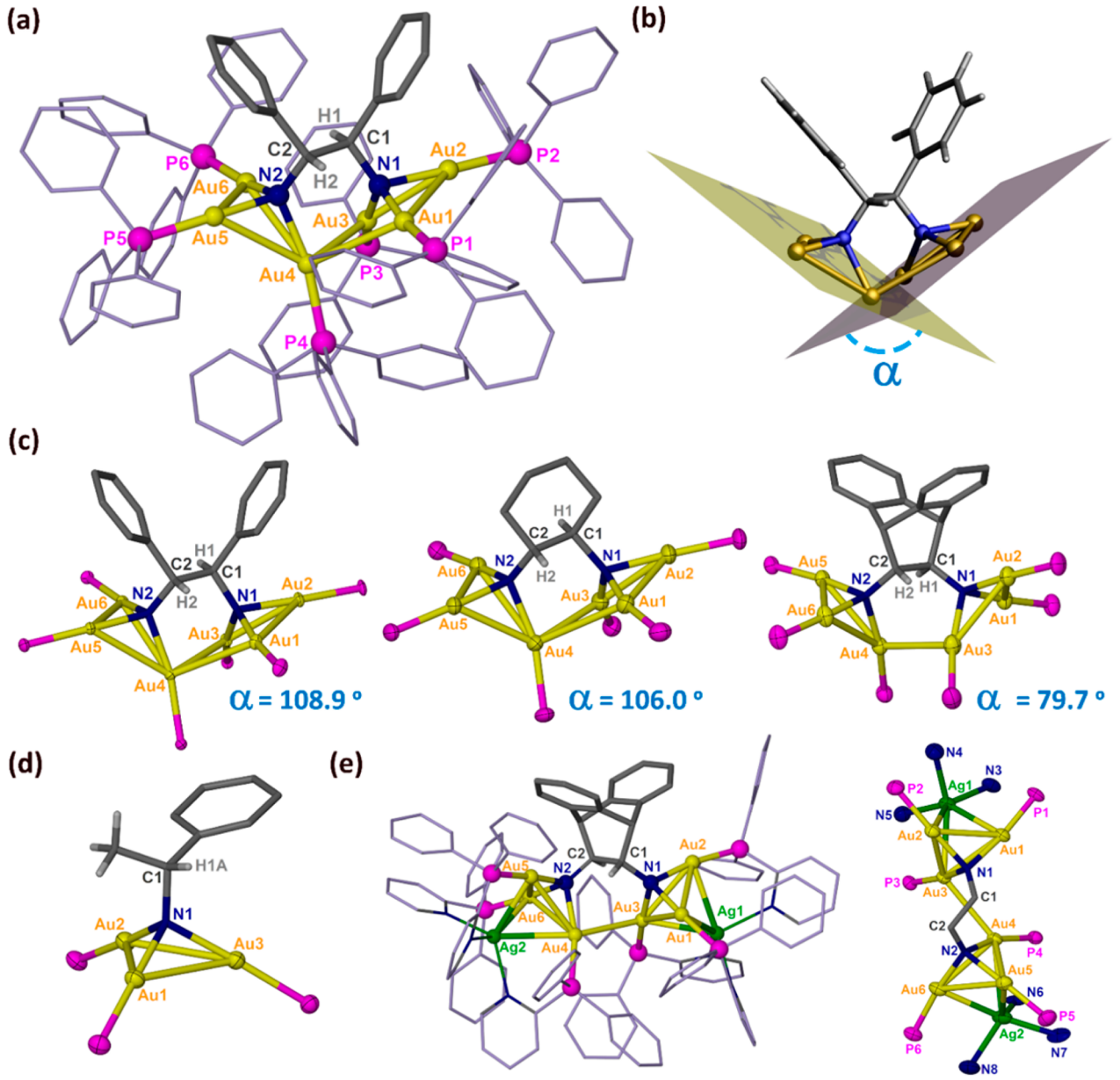

Figure 2. Crystal structures of complexes **1**−**5**. (a) Detailed structure of complex **1**-(*R*,*R*) with tetrafluoroborate anions and solvent molecules omitted for clarity. (b) Schematic diagram for the dihedral angle (α) determined by two Au_3 planes. (c) Gold-diimido core structures of **1**-(*R*,*R*), **2**-(*R*,*R*), and **3**-(*R*,*R*). (d) Core structure of **4**-(*rac*) with only one enantiomer of L^4 shown here. (e) Crystal structure of **5**-(*rac*). Only one enantiomer of L^3 is shown here. Color coding: yellow, Au; green, Ag; black, C; gray, H; blue, N; purple, P; light violet, C atoms in PPh_3 and dppy ligands.

three gold atoms with the Au−N distances ranging from 2.044(10) to 2.065(10) Å, comparable to the values in previously reported gold−imido complexes.[20] The Au···Au distances (3.071(1)−3.144(1) Å) of the Au1−Au2−Au3 triangle are shorter than twice the van der Waals radius of the gold atom (3.4 Å), clearly suggesting the presence of the attractive aurophilic interaction.[21] As to three PPh_3 ligands in **4**, the arrangements of phenyl rings are all in a propeller-like *P*-form corresponding to the central L^4-(*R*) ligand (Figure S1), highlighting the possible contribution of the phosphine ligands to the chirality of the whole complex.

Relative to the frequent use of monoamine derivatives for the synthesis of gold−imido clusters,[20] there are no precedent examples using 1,2-diamine ligands to achieve higher nuclearity gold clusters. In our study, the enantiomers of the 1,2-diamine ligands (H_4L^1, H_4L^2, and H_4L^3) can readily react with $[Au_3O]$ in stoichiometric ratio to yield gold cluster complexes **1**−**3**, respectively. Generally, as compared to the crystallization of racemic complexes, it is much harder to crystallize enantiopure complexes due to the lack of reflection and inversion symmetry in molecular packing. To our delight, we can achieve a high yield of 86%, 82%, and 89% for obtaining crystals of **1**-(*R*,*R*), **2**-(*R*,*R*), and **3**-(*R*,*R*), respectively. X-ray crystallographic analysis revealed that **1**-(*R*,*R*), **2**-(*R*,*R*), and **3**-(*R*,*R*) all crystallize in a chiral space group of *P*1, $P2_12_12_1$, and $P2_1$, respectively. The low Flack parameters of 0.010(6) for **1**-(*R*,*R*), 0.076(12) for **2**-(*R*,*R*), and 0.019(10) for **3**-(*R*,*R*) indicate a homochiral molecular packing in these crystals. **1**-(*R*,*R*), **2**-(*R*,*R*), and **3**-(*R*,*R*) are almost isostructural and have a common molecular formula of $[(AuPPh_3)_6(L^n\text{-}(R,R))](BF_4)_2$ (n = 1, 2, and 3). As shown in Figure 2a−c, crystal structures of **1**-(*R*,*R*), **2**-(*R*,*R*), and **3**-(*R*,*R*) all comprise a tetraanionic unit L^n-(*R*,*R*), two

DOI: 10.1021/jacs.6b01658
J. Am. Chem. Soc. 2016, 138, 5634−5643

tetrafluoroborates plus six $AuPPh_3$ units. Each $\mathbf{L}^n$-(*R,R*) anion adopts a μ_6-η^3,η^3 mode to bind with six gold(I) atoms by means of two μ_3-imido nitrogen centers. The Au−N bond distances in three such complexes are similar and within the range of 2.018(14)−2.103(11) Å. However, the Au···Au contacts in these three chiral clusters are distinct. The Au···Au distances in the NAu_3 aggregates of **1**-(*R,R*) lie in the range of 2.882(1)−3.206(1) Å, shorter than the values of **2**-(*R,R*) (2.898(1)−3.348(1) Å) and **3**-(*R,R*) (2.970(1)−3.310(1) Å). In addition, two NAu_3 aggregates held by the same $\mathbf{L}^n$ ligand in every chiral cluster complex are linked by single or double Au···Au contacts. In **1**-(*R,R*), there are two contacts between the NAu_3 aggregates at Au3···Au4 = 3.054(1) Å and Au1···Au4 = 3.188(1) Å. Two similar Au···Au contacts in **2**-(*R,R*) are found to be elongated to 3.082(1) and 3.386(1) Å. In contrast, only one Au···Au contact at Au3···Au4 = 3.036(1) Å is observed between two NAu_3 aggregates in **3**-(*R,R*). Along the shortest aurophilic connections, the gold chain Au1−Au2−Au3−Au4−Au5−Au6 constitutes a sigmoidal pattern in **1**-(*R,R*) and **2**-(*R,R*), but a reversed S-shaped one in **3**-(*R,R*). It is remarkable that such six interacting gold atoms in **1**−**3** are not coplanar and thus form an asymmetric arrangement as shown in Figure 1a. A characteristic dihedral angle α defined by two Au_3 planes in **1**−**3** varies from 108.9° through 106.0° to 79.7°. These special arrangements of the gold atoms in **1**−**3** are in good agreement with the C_2-symmetric positioning of two imido centers in the $\mathbf{L}^n$-(*R,R*) ligands, wherein the N1−C1−C2−N2 torsion angle gradually increases from 57.4° in **1** through 67.1° in **2** to 97.1° in **3** and the N1−N2 distance extends from 2.921 Å through 3.008 Å to 3.323 Å. The Au_6 cluster aggregates in **1**−**3** are all peripherally surrounded by six coordinative PPh_3 ligands. In sharp contrast to the ordered chiral arrangements of the phenyl rings of PPh_3 in **4**, the occurrence of *P*- or *M*-form propeller-like arrangements for the phenyl rings in **1**−**3** is random (Figures S2−S4). For instance, three PPh_3 in *P*-form and three in *M*-form coexist in **1**-(*R,R*), while two in *P*-form and four in *M*-form are found in **2**-(*R,R*) and **3**-(*R,R*).

In view of the paucity of systematic investigations on the chirality of heterometallic clusters,[22] we next extended the above synthetic protocol to a mixed metal system. Equally importantly, we attempted to fix the arrangement of the aromatic rings in the phosphine ligand to evaluate the contribution of phosphine ligands to the chirality of the whole cluster complex. The mixed gold−silver cluster $[OAu_3Ag(dppy)_3](BF_4)_2$ (dppy = diphenylphosphino-2-pyridine)[23] with the conformation of dppy fixed by silver coordination was then employed to replace $[\mathbf{Au_3O}]$ in the synthetic procedures for **1**−**3**. Unfortunately, the reaction of $[OAu_3Ag(dppy)_3](BF_4)_2$ with $\mathbf{H_4L^1}$ or $\mathbf{H_4L^2}$ led to a mixture of many species as evidenced in mass spectroscopy. Finally, racemic $\mathbf{H_4L^3}$ reacted with $[OAu_3Ag(dppy)_3](BF_4)_2$ to generate a major product **5**-(*rac*), which crystallizes in a centrosymmetric space group *C*2/*c* in 90% yield. The molecular formula of **5**-(*rac*) was determined as $[(Au_6Ag_2(\mathbf{L^3}\text{-}(\mathbf{R,R}))(dppy)_6)(Au_6Ag_2(\mathbf{L^3}\text{-}(\mathbf{S,S}))(dppy)_6)](BF_4)_8$. Each cluster unit comprises an enantiomer of $\mathbf{L}^3$, six gold atoms, two silver atoms, plus six dppy ligands (Figure 2e). The $\mathbf{L}^3$ ligand in the μ_6-η^3,η^3 mode is surrounded by six gold atoms (Au−N, 2.029(8)−2.125(10) Å; Au···Au, 2.963(1)−3.308(1) Å) as well as the scenario in the structure of **3**-(*R,R*). It is notable that sigmoidal and reverse-sigmoidal hexanuclear gold cluster motifs explicitly determined by a $\mathbf{L}^3$-(*R,R*) or $\mathbf{L}^3$-(*S,S*) ligand coexist in the structure of **5**-(*rac*). In addition, each Au_3 triangle around an imido center is further capped by a silver atom through Au···Ag interactions (2.868(1)−3.119(1) Å). The opposite side of the silver atom coordination sphere is occupied by three pyridyl nitrogen atoms of the dppy ligands (Ag−N: 2.338(11)−2.409(15) Å). The N−C−C−N torsion angles and the N−N distances of $\mathbf{L}^3$ in **5**-(*rac*) are measured as 97.7−99.9° and 3.296−3.358 Å, respectively, which are comparable with the values in **3**-(*R,R*). However, relative to the PPh_3 arrangements in **3**-(*R,R*), the dppy ligands attached on the same $[Au_3Ag]$ unit are arranged in a more compact and ordered form due to the coordination of silver atoms. The arrangements of the aromatic rings in dppy of **5** can be classified into two scenarios (Figure S5). First, three pyridine rings around the same silver atom form a triblade propeller chiral conformation (Λ or Δ). Second, three dppy ligands around a $[Au_3Ag]$ aggregate all adopt the same *P*- or *M*-form. Between two $[Au_3Ag]$ subunits within a $[(dppy)_6Au_6Ag_2\text{-}\mathbf{L^3}]$ unit, the above-mentioned asymmetric arrangements of three pyridine rings around a silver atom and configurations of the dppy ligands are totally opposite.

Complexes **1**−**5** can keep their structures intact in solution as evidenced by high-resolution ESI mass spectrometry and NMR. The solution samples for ESI−MS analysis were prepared by dissolving the crystalline solids of **1**−**5** in suitable solvents. A series of isotopically well-resolved peaks are observed, and they can be assigned to the corresponding cluster complex minus one or two BF_4^- species (Figures S6−S10). The ^{31}P and ^1H NMR spectra of **1**−**5** were collected to gain deep insight into their structures in solution. The ^{31}P NMR spectrum of **4** gives a single peak at δ = 29.5 ppm, and three sets of multiplet signals corresponding to the three discernible protons of phenyl rings of PPh_3 are explicitly observed (Figure S11). These results agree well with the NMR spectra of the reported trinuclear gold−imido cluster complexes.[20a,b] In contrast, the ^{31}P NMR spectra of **1**−**3** reveal five or six peaks in the range of 27.5−31.0 ppm (Figures S12−S14). Meanwhile, very complicated proton NMR spectra for **1**−**3** are obtained, which comprise several sets of multiplets within the range of 6.9−7.6 ppm. We speculate that six nonequivalent PPh_3 ligands and the restricted rotation of phenyl rings of PPh_3 due to steric hindrance both account for the intricate NMR spectra of **1**−**3**. Upon fixing the aromatic rings of the phosphine ligand by the coordination of silver atoms, complex **5** exhibits a broad peak at 32.4 ppm in the ^{31}P NMR spectrum and several broad multiplets in the proton NMR spectrum (Figure S15).

Circular Dichroism Spectra of 1−5. All enantiopure samples of **1**−**5** for CD measurements were synthesized as crystalline solids based on the above synthetic procedures. Commercially available enantiomers of $\mathbf{H_4L}^n$ (n = 1−3) and $\mathbf{H_2L^4}$ were used as starting materials. The composition and purity of these samples were evidenced by elemental analysis. The chloroform solutions of **1**−**4** and the dichloromethane solution of **5** were employed for CD measurements. As shown in Figure 3, the CD spectra of the enantiomers of **1**, **2**, **3**, and **5** all show an intense Cotton effect and an excellent mirror image relationship in the 250−500 nm range, whereas the same concentrated solution of **4** gives almost negligible CD response. Taking into account the fact that the CD spectra of chiral diamines $\mathbf{H_4L}^n$ (n = 1−3) give very weak response within this range, the intense CD responses of **1**, **2**, **3**, and **5** possibly arise from metal-based electronic transitions. The CD spectrum of **1**-(*R,R*) reveals three signals: 273 (−), 316 (−), and 372 (+) nm. **2**-(*R,R*) has four intense CD signals at 254 (+), 278 (−), 311 (−), and 373 (+) nm. Three unambiguous signals at 257 (+),

DOI: 10.1021/jacs.6b01658
J. Am. Chem. Soc. 2016, 138, 5634−5643

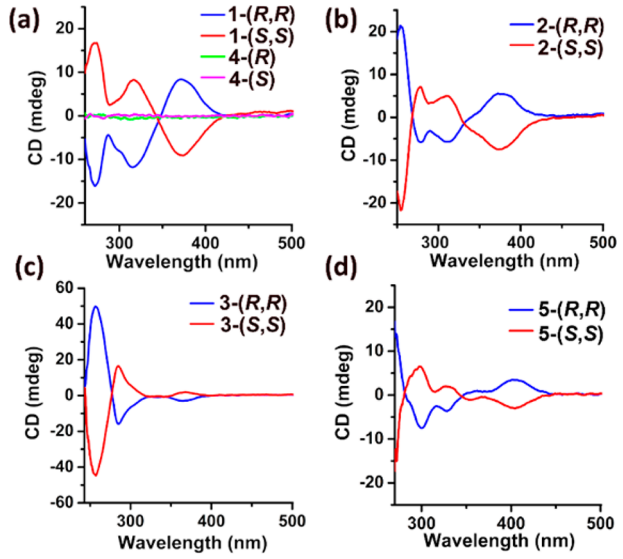

Figure 3. CD spectra of enantiopure metal cluster complexes **1**−**4** in $CHCl_3$ ($c = 2.5 \times 10^{-5}$ M) and **5** in CH_2Cl_2 ($c = 2.5 \times 10^{-5}$ M). The spectra of **1** and **4** are shown together for contrast.

285 (−), and 365 (−) nm are observed in the CD spectrum of **3**-(***R,R***). It is noteworthy that the Cotton effect of **1** and **2** at the low energy region is opposite to that of **3**. This observation seemingly corresponds to a sigmoidal gold arrangement in **1** and **2** but a reverse one in **3**. The heteronuclear Au−Ag cluster complex **5**-(***R,R***) exhibits four CD signals at 300 (−), 329 (−), 355 (+), and 402 (+) nm.

To systematically evaluate the CD intensity of **1**−**5**, anisotropy factors over the spectral range are calculated on the basis of the equation $g = \Delta A/A = \theta[\text{mdeg}]/(32\,980 \times A)$ (Figure 4). The anisotropy factors for **1**, **2**, **3**, and **5** increase with increasing wavelengths. Despite only 6−8 metal atoms being included in the structures of **1**−**3** and **5**, their CD anisotropy factors are surprisingly strong with values up to 6×10^{-3}, among the largest values for gold clusters and nanoclusters up to now.[9] As compared to the anisotropy factors of **1**−**3** and **5**, the *g* value for the trinuclear gold−imido cluster complex **4** is very small below 320 nm. Above this wavelength, the calculated *g* value is not reliable because the absorption of **4** steeply descends to zero.

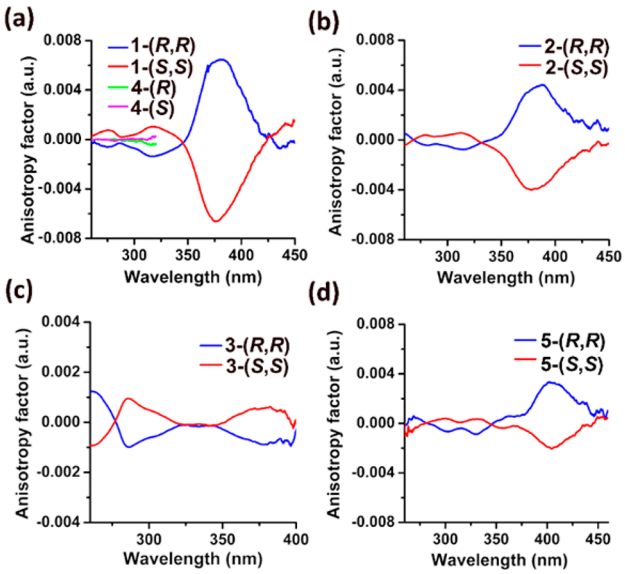

Figure 4. Anisotropy factors of enantiopure cluster complexes of **1**−**5**. The calculation of the anisotropy factors for **4**-(***R***) and **4**-(***S***) is cut off at 320 nm.

DISCUSSION

Geometrically, there are three structural factors contributing to the chirality of the cluster complexes **1**−**5**, which include the chiral di- or monoimido ligand $\mathbf{L}^n$ (n = 1−4), the asymmetrically arranged metal cluster, and the chiral arrangement of aromatic rings of phosphine ligands. Because the $\mathbf{L}^4$ ligand in the monoimido Au_3 cluster complex **4** can be roughly considered as one-half of the $\mathbf{L}^1$ in the diimido Au_6 cluster complex **1**, we thus make a direct structural comparison of **1** and **4** based on their crystal structures and correlate it with their corresponding CD responses. First, the bare gold triangle in **4** has a mirror image symmetry, while the sigmoidally arranged Au_6 cluster in **1** is intrinsically chiral. Theoretically, the asymmetric Au_6 cluster in **1** should provide a more significant contribution to the CD response than the Au_3 triangle in **4**. In addition, scrutiny of crystal structures of **1** and **4** has shown that the phenyl rings of PPh_3 are all arranged in the same chiral pattern in **4** but in a random *P*- and *M*-form in **1**. The chirality contribution from such asymmetric arrangements in **4** should be larger than the random arrangements in **1**. However, the measured CD response of **1** (g up to 6×10^{-3}) is much stronger than that of **4** as evidenced by anisotropy factors (Figure 4). These results imply that the asymmetric arrangements of phenyl rings cannot generate an intense CD response in the present system and the CD response difference between **1** and **4** may be mostly from the asymmetrically arranged Au_6 cluster aggregate in **1**. It is necessary to point out that the present structural comparison is based on the crystalline solid structures of **1** and **4**, while the measurement of CD spectra is aimed at the solution samples. Previous investigation by Bürgi and co-workers has confirmed that the conformations of ligands on the surface of chiral gold nanoclusters are different in solution and in solid state.[24] Therefore, we cannot totally rule out the chirality contribution of the PPh_3 ligands in **1** to the CD response because the phenyl rings of PPh_3 may constitute an ordered and asymmetric arrangement in solution. However, the small anisotropy factor of **4** that contains a chiral pattern of PPh_3 suggests that the asymmetric arrangements of phenyl ring in PPh_3 may not lead to an intense CD response.

To gain further insight into the prominent difference of CD response for **1** and **4**, we conducted a simulation of their UV−vis and CD spectra and detailedly analyzed transition-related HOMO and LUMO orbitals in the 250−500 nm range (Figure 5, Figures S16−S21). As shown in Figure 5a and Figure S16, the calculated UV−vis spectra of complexes **1**−**5** agree quite well with the measured spectra. The excellent data fit between experimental and calculated UV−vis spectra not only signifies the validity of the present calculation methods, but also suggests a small difference between the structures of **1**−**5** in solution and in the solid state as the calculated UV−vis spectra were conducted on the basis of single-crystal structures. Because CD spectroscopy actually measures the difference in absorbance of left- and right-circularly polarized light by gold cluster complexes, the contribution of different structural motifs to the electronic transition-related HOMO and LUMO orbitals could be correlated with their influence on CD response. The CD signals at the lowest energy region, which mostly exhibit

DOI: 10.1021/jacs.6b01658
J. Am. Chem. Soc. 2016, 138, 5634−5643

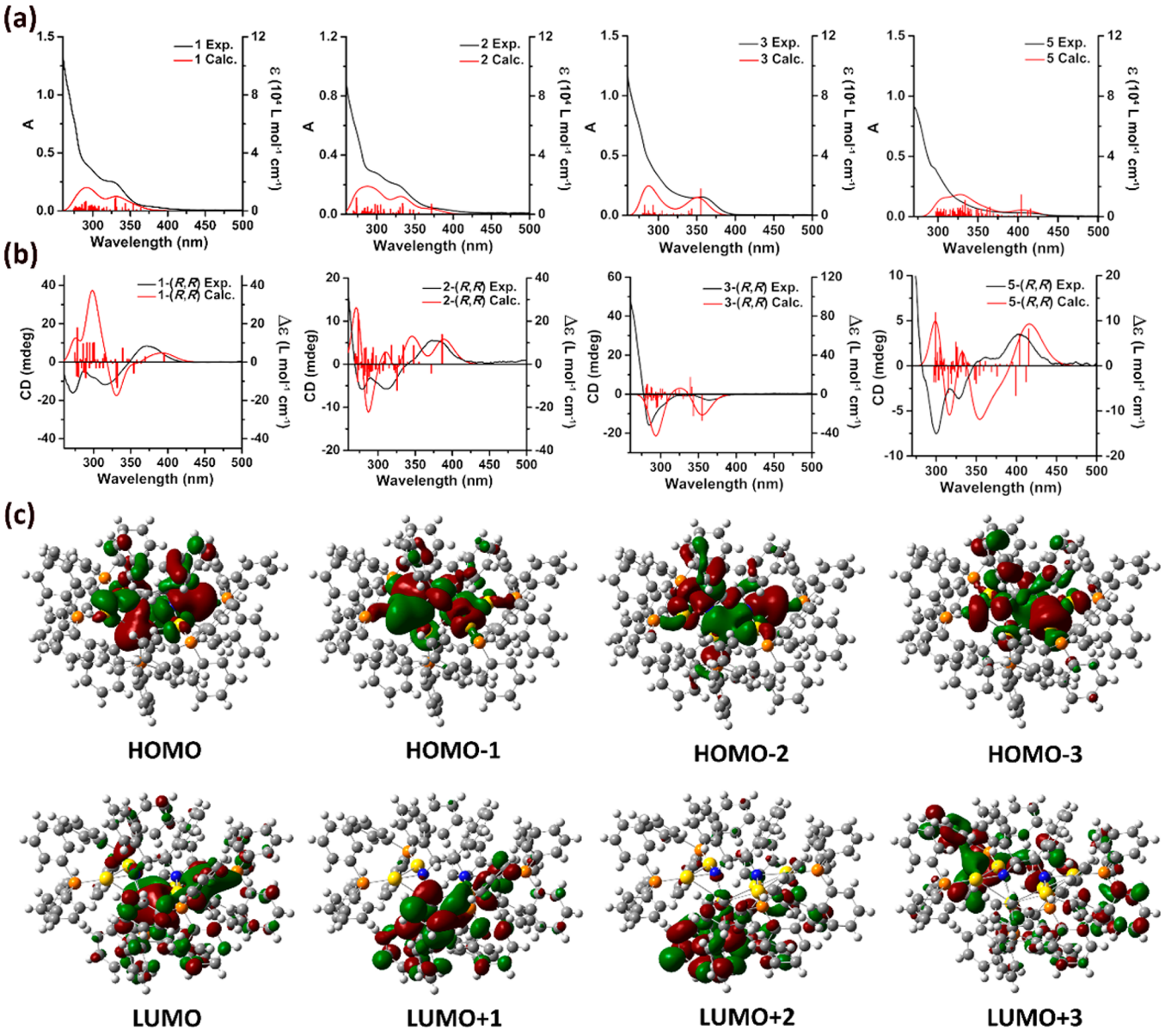

Figure 5. (a) Experimental (black line) and calculated (red line for calculated spectra and red columns for oscillator strength in au) UV−vis absorption spectra for **1**, **2**, **3**, and **5**. (b) Experimental (black line) and calculated (red line for calculated spectra and red columns for rotatory strength in au) CD spectra for **1**-(*R*,*R*), **2**-(*R*,*R*), **3**-(*R*,*R*), and **5**-(*R*,*R*). (c) Plots of near-frontier transition-related orbitals of **1**-(*R*,*R*).

the largest anisotropy factors, are selected for detailed analysis. The measured CD spectrum of **4** shows a relatively apparent response around 310 nm (Figure S16). TD-DFT calculations indicate that this absorption band can be mainly ascribed to the transitions of HOMO → LUMO/LUMO+1. On the basis of Mulliken population analysis (Table S1), we found the HOMO orbital primarily lies on the gold atoms and the $\mathbf{L}^4$ ligand, and the LUMO to LUMO+3 orbitals mostly arise from the phenyl groups of PPh_3. Because the bare Au_3 triangle in **4** is symmetric, we conjecture that the chiroptical activity of **4** primarily arises from the $\mathbf{L}^4$ ligand and the chiral arrangement of phenyl rings of PPh_3. In consideration of the very small anisotropy factors of **4**, we infer that these two structural motifs are not able to produce a strong CD response. On the other hand, DFT simulations of the CD spectrum of **1**-(*R*,*R*) have identified that the intense CD signal at 372 nm ($g = 6 \times 10^{-3}$) in the measured CD spectrum is derived from the transitions out of HOMO into LUMO−LUMO+6. Mulliken population analysis revealed that the HOMO orbital of **1** lies mainly on the six-membered gold cluster and the $\mathbf{L}^1$ ligand (especially the two imido nitrogen atoms) and the transition-related LUMO to LUMO+*n* orbitals mostly locate on the phenyl groups of PPh_3 (Figure 5c). In view of the random arrangements of the phenyl rings of PPh_3 in **1**, we consider that the CD responses of **1** mainly originate from the contribution of asymmetrically arranged gold clusters and the $\mathbf{L}^1$ ligand. The mechanism of CD responses related to the electronic state mixing of the ligands and gold clusters was also proposed in chiral Au_{25} clusters by Jin et al.[25] Considering the weak CD response of **4** originated from the $\mathbf{L}^4$ ligand and the chiral arrangement of phenyl rings, we further conceive that the strong CD response of **1** is mostly dominated by the sigmoidal gold cluster rather than the central $\mathbf{L}^1$ ligand.

We next embark on the structural comparison and electronic transition analysis of **1**-(*R*,*R*), **2**-(*R*,*R*), and **3**-(*R*,*R*) to elucidate the biased influence of asymmetrically arranged gold

DOI: 10.1021/jacs.6b01658
J. Am. Chem. Soc. 2016, 138, 5634−5643

clusters and the central diimido ligands on the chiroptical property. As summarized in the structural description, the absolute configurations of the diimido ligands $\mathbf{L}^n$ (n = 1−3) in the crystal structures of **1**-(***R,R***), **2**-(***R,R***), and **3**-(***R,R***) are the same, while the arrangements of six gold atoms are different in **1**−**3**. Along the shortest aurophilic connections, the gold chain Au1−Au2−Au3−Au4−Au5−Au6 constitutes a sigmoidal pattern in **1**-(***R,R***) and **2**-(***R,R***), but a reversed S-shaped one in **3**-(***R,R***). On the basis of the measured CD spectra, the CD signals with the largest anisotropy factors for **1**-**3**-(***R,R***) are at 372 (+), 373 (+), and 365 (−) nm, respectively. Theoretical simulations of the CD spectrum of **1**-(***R,R***) reveal that the transitions out of HOMO into LUMO/LUMO+1 (395 nm) and into LUMO−LUMO+6 (369 nm) both have moderate positive rotatory strengths to produce the overall positive Cotton effect at 372 nm. As to complex **2**-(***R,R***), the transition of HOMO → LUMO/LUMO+1 at 386 nm with strong positive rotatory strengths dominates the positive Cotton effect at 373 nm in the measured CD spectrum. Furthermore, four transition pathways out of HOMO have been found to account for the negative CD response at 365 nm in the measured CD spectrum of **3**-(***R,R***). Two of them possess moderate positive rotatory strength, while the other two exhibit strong negative strength, which in total show a negative Cotton effect. On the basis of Mulliken population analysis, the HOMO and near-frontier HOMO−n orbitals of **1**−**3** all lie mainly on the six-membered gold clusters and the two imido nitrogen atoms of the $\mathbf{L}^n$ ligands. In addition, the transition-related LUMO to LUMO+n orbitals have been found to mostly arise from the phenyl groups of PPh_3. Thus, on the basis of the structural comparison and calculation results, the chiroptical activity of **1**−**3** can be ascribed to the asymmetrically arranged gold clusters and the $\mathbf{L}^n$ ligands. In addition, in view of the same absolute configuration of the $\mathbf{L}^n$ (n = 1−3) ligands in **1**−**3**, we deduce that the asymmetrically arranged gold clusters play a pivotal role in determining the CD response of complexes **1**−**3**. This observation is in agreement with the theoretical investigations reported by Govorov and co-workers, which systematically evaluated the influence of chiral nanocrystals with various chiral shapes on the CD response.[26] In addition, this assessment provides a good rationale for the opposite Cotton effect between **1**/**2** and **3** at the low energy region corresponding to the S-shaped arrangement of Au_6 clusters in **1** and **2** and the reverse S-shaped in **3**. Our present finding constitutes a sharp contrast to the theoretical investigation on the chirality origin of the gold nanocluster $[Au_{11}(BINAP)_4X_2]^+$.[27] In that work, Aikens and co-workers found the perpherial phosphorus ligands rather than the metal core have a strong effect on intensity of CD signals. In view of the spherical structure of the Au_{11} core in $[Au_{11}(BINAP)_4X_2]^+$ and the elongated conformation of the Au_6 cluster in **1**−**3**, we conjecture that the geometric shape of metal NCs may also influence the CD response, which should be seriously studied in the future.

To further substantiate the major influence of the asymmetric arrangements of gold clusters on the chiroptical properties, we built a simplified Au_6 cluster model for mimicking the structural variation of the Au_6 clusters in **1**−**3**. The cluster model consists of six Au(0) atoms to remove the influence of required negatively charged ligands in Au(I) clusters, wherein two Au_3 triangles are connected by two Au···Au contacts at Au1−Au4 and Au3−Au4 (Figure 6a). All Au···Au distances are set as 2.85 Å, a typical distance for aurophilic

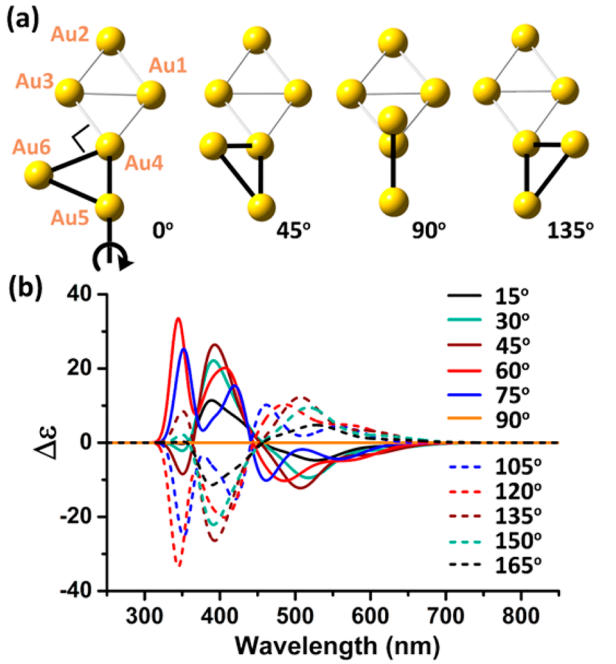

Figure 6. (a) Structures of the Au_6 cluster model with varied dihedral angles determined by the Au1−Au2−Au3 and Au4−Au5−Au6 planes. All Au−Au distances are set as 2.85 Å. (b) Calculated CD spectra of the Au_6 cluster model upon the variation of the dihedral angle from 15° to 165°.

interaction. A dihedral angle defined by the two Au_3 triangles is tailored to achieve a nonplanar sigmoidal or reverse-sigmoidal gold cluster similar to the scenarios in the crystal structures of **1**−**3**. As shown in the simulated CD spectra (Figure 6b), the escalating of the dihedral angles from 0 to 45° formally enhances the asymmetry of the gold clusters and thus increases the intensity of CD peaks at around 350 (**I**), 400 (**II**), and 500 (**III**) nm. Further varying the angles from 45° to 90° engenders the intensity decreasing and the positional change of peaks **II** and **III**. Meanwhile, it is noteworthy that the Cotton effect of peak **I** is reversed upon the variation of the dihedral angle from 45° to 90°. When a supplementary dihedral angle such as 135° is adopted, its simulated CD spectrum is totally mirror image-related to the spectrum of the Au_6 cluster with a dihedral angle of 45°. The simulation results reproduce the Cotton effect variation for **1**-**3**-(***R,R***) (especially at the low energy region: 372 nm (+) for **1**-(***R,R***), 373 nm (+) for **2**-(***R,R***), and 365 nm (−) for **3**-(***R,R***)) and provide supportive evidence to correlate the CD responses with the S-shaped Au_6 clusters in **1** and **2** and the reverse S-shaped in **3**.

Furthermore, we also conducted the simulation of UV−vis and CD spectra of the heteronuclear cluster complex **5** (Figure 5a,b). As shown in the crystal structure of **5**, the two $[Au_3Ag]$ aggregates are linked by a Au···Au contact to generate a sigmoidal Au_6 arrangement corresponding to the enantiomer $\mathbf{L}^3$-(***S,S***). The two Au_3 planes constitute a dihedral angle of 73.7−75.5°. Meanwhile, the chiral arrangements of three pyridine rings around a silver atom and three aromatic rings of a dppy ligand within a $[Au_6Ag_2(\mathbf{L}^3)(dppy)_6]$ are in *meso* form in **5**. The involvement of two more silver atoms within the core cluster aggregate makes the maximum absorption wavelength of **5** extend to 410 nm in the measured UV−vis spectrum, which is in good agreement with the calculated band at 415 nm. Theoretical calculations reveal that this absorption

DOI: 10.1021/jacs.6b01658
J. Am. Chem. Soc. 2016, 138, 5634−5643

band arises from a combination of several transitions out of HOMO to HOMO−3. Mulliken population analysis explores that the transition-related HOMO and HOMO−*n* orbitals of **5** are mainly located on the L^3 ligand plus a moderate contribution of the six gold atoms. The contribution of silver atoms is quite small. The near-frontier LUMO to LUMO+3 orbitals of **5** have been found to mostly arise from the phosphine ligand dppy. We therefore envision that the mechanism of the electronic transitions of **5** is complicated. It may include both interligand and metal-to-ligand charge transfer. In view of the *meso* form of the arrangements of the aromatic rings of dppy in **5**, we ascribe the complex CD spectrum of **5** to the influence of the L^3 ligand and six asymmetrically arranged gold atoms. As compared to the CD spectrum of **3**-(*R*,*R*), **5**-(*R*,*R*) has evidently different CD response including the absorption region and Cotton effects despite involving the same L^3-(*R*,*R*) ligand. These results indicate that the introduction of additional metal ions and different peripheral ligands can act as an alternative way to regulate the CD response of resulting metal clusters.

CONCLUSIONS

In summary, we have accomplished the synthesis of a series of five enantiopure metal clusters based on chiral amine ligands. Structural characterization revealed the formation of sigmoidally and reverse-sigmoidally arranged gold clusters upon the use of chiral diamine ligands with the same absolute configuration. Such chiral gold clusters give strong CD response with the anisotropy factor up to 6×10^{-3}. Theoretical calculations revealed that the strong CD responses are closely related to the gold cluster-dominated HOMO orbitals, thus correlating the CD responses with the geometrical arrangement of gold atoms. This study showcases a promising approach to build up a platform to investigate the structure and chiroptical property relationship of chiral metal clusters at atomic level. Structure and CD response comprehension of these small chiral metal clusters foresees deep research in understanding the origin of chirality in metal NCs and stimulates the advancement of designing novel chiroptical functional materials.

EXPERIMENTAL SECTION

All commercially available chemicals were used without further purification. The solvents used in this study were dried by standard procedures. All reactions were carried out under a nitrogen atmosphere unless otherwise noted. $[O(AuPPh_3)_3]BF_4$[19] and $[OAu_3Ag(dppy)_3](BF_4)_2$[23] were prepared according to the published methods. ^1H and ^{31}P NMR experiments were carried out on a JEOL ECX-400 MHz instrument. Synthetic methods for the enantiopure cluster complexes of **1**−**5** were identical with the methods described below with commercially available enantiomers of H_4L^n (n = 1−3) and H_2L^4 as starting materials.

Synthesis of $[(AuPPh_3)_6(L^1$-(*R*,*R*))$](BF_4)_2$ (1-(*R*,*R*)). (1*R*,2*R*)-1,2-Diphenylethylenediamine (H_4L^1-(*R*,*R*)) (2.3 mg, 0.011 mmol) in 2 mL of CH_2Cl_2 was added to a CH_2Cl_2 (2 mL) solution of $[O(AuPPh_3)_3]BF_4$ (29.6 mg, 0.02 mmol) under vigorous stirring. The solution underwent a gradual color change from colorless to bright yellow. After 10 h, removing the solvent finally gave an oily yellow crude product. Yellow block crystals of **1**-(*R*,*R*) were acquired by diffusion of diethyl ether into the concentrated CH_3OH solution of **1**-(*R*,*R*). Yield: 86% (27.0 mg). Anal. Calcd for $[(AuPPh_3)_6(L^1$-(*R*,*R*))$](BF_4)_2$ ($C_{122}H_{102}Au_6B_2F_8N_2P_6$): C, 46.71; H, 3.28; N, 0.89. Found: C, 46.56; H, 3.51; N, 0.77.

Synthesis of $[(AuPPh_3)_6(L^2$-(*R*,*R*))$](BF_4)_2$ (2-(*R*,*R*)) and $[(AuPPh_3)_6(L^3$-(*R*,*R*))$](BF_4)_2$ (3-(*R*,*R*)). The synthesis of **2**-(*R*,*R*) and **3**-(*R*,*R*) is according to the synthetic procedure for **1**-(*R*,*R*) with (1*R*,2*R*)-1,2-diaminocyclohexane (H_4L^2-(*R*,*R*)) and (11*R*,12*R*)-9,10-dihydro-9,10-ethanoanthracene-11,12-diamine (H_4L^3-(*R*,*R*)) in place of H_4L^1-(*R*,*R*). Yellow block crystals of **2**-(*R*,*R*) were obtained by diffusion of diethyl ether into its concentrated CH_2Cl_2 solution. Yield: 82% (24.9 mg). Anal. Calcd for $[(AuPPh_3)_6(L^2$-(*R*,*R*))$](BF_4)_2 \cdot (H_2O)_2$ ($C_{114}H_{104}Au_6B_2F_8N_2O_2P_6$): C, 44.52; H, 3.41; N, 0.91. Found: C, 44.22; H, 3.35; N, 0.77. Colorless plate crystals of **3**-(*R*,*R*) were acquired by diffusion of diethyl ether into the concentrated $CHCl_3$ solution of **3**-(*R*,*R*). Yield: 89% (28.1 mg). Anal. Calcd for $[(AuPPh_3)_6(L^3$-(*R*,*R*))$](BF_4)_2 \cdot (CHCl_3)$ ($C_{125}H_{103}Au_6B_2Cl_3F_8N_2P_6$): C, 45.76; H, 3.16; N, 0.85. Found: C, 45.54; H, 2.80; N, 1.08.

Synthesis of $[(AuPPh_3)_3(L^4$-(*rac*))$](BF_4)$ (4-(*rac*)). (±)-1-Phenylethylamine (H_2L^4-(*rac*)) (12.1 mg, 0.1 mmol) in 2 mL of THF was added to a THF (2 mL) suspension of $[O(AuPPh_3)_3]BF_4$ (29.6 mg, 0.02 mmol) under vigorous stirring. The suspension turned clear within 0.5 h. Evaporation of solvent produced an oily crude product in light yellow. Colorless plate crystals of **4**-(*rac*) were acquired by layering diethyl ether onto the concentrated THF solution of **4**-(*rac*). Yield: 69% (21.9 mg). Anal. Calcd for $[(AuPPh_3)_3(L^4$-(*rac*))$](BF_4)$-$(C_{62}H_{54}Au_3BF_4NP_3)$: C, 47.02; H, 3.44; N, 0.88. Found: C, 47.13; H, 3.37; N, 1.06.

Synthesis of $[Au_6Ag_2(L^3$-(*rac*))$(dppy)_6](BF_4)_4$ (5-(*rac*)). The synthesis of **5**-(*rac*) is based on the synthetic procedure for **3**-(*R*,*R*) with $[OAu_3Ag(dppy)_3](BF_4)_4$ (dppy = diphenylphosphino-2-pyridine) in place of $[O(AuPPh_3)_3]BF_4$. Yellow plate crystals of **5**-(*rac*) were obtained by layering diethyl ether onto the concentrated CH_2Cl_2 solution of **5**-(*rac*). Yield: 90% (32.0 mg). Anal. Calcd for $[Au_6Ag_2(L^3$-(*rac*))$(dppy)_6](BF_4)_4$ ($C_{118}H_{96}Ag_2Au_6B_4F_{16}N_8P_6$): C, 39.85; H, 2.72; N, 3.15. Found: C, 40.09; H, 2.94; N, 3.30.

CD and UV−Vis Spectroscopy. CD and UV−vis measurements were carried out on a Jasco J-810 circular dichroism spectropolarimeter at room temperature. Predried and distilled methylene chloride and chloroform were used as solvents. For the CD measurements, four accumulations of standard sensitivity at the scan rate of 100 nm/min and data pitch of 0.2 nm were averaged. Anisotropy factors were calculated according to $g = \theta[\text{mdeg}]/(32\,980 \times A)$ using the UV−vis spectrum data measured by the CD spectrometer.

X-ray Crystallography. Single-crystal X-ray data for complexes **1**−**5** were collected at 173 K with Mo Kα radiation (λ = 0.71073 Å) on a Rigaku Saturn 724/724+ CCD diffractometer with frames of oscillation range 0.5°. The selected crystal was mounted onto a nylon loop by polyisobutene and enveloped in a low-temperature (173 K) stream of dry nitrogen gas during data collection. The absorption corrections were applied using multiscan methods. All structures were solved by direct methods, and non-hydrogen atoms were located from difference Fourier maps. Non-hydrogen atoms were subjected to anisotropic refinement by full-matrix least-squares on F^2 by using the SHELXTL program unless otherwise noticed.[28] CCDC numbers for reported complexes are 1449580 (**1**-(*R*,*R*)), 1449581 (**2**-(*R*,*R*)), 1449592 (**3**-(*R*,*R*)), 1449642 (**4**-(*rac*)), and 1449659 (**5**-(*rac*)).

Computational Methods. Theoretical calculations of complexes **1**−**5** and Au_6 model clusters were performed using the Gaussian 09 program.[29] Structures of **1**−**5** for calculation were built up on the basis of single-crystal structures. Becke three-parameter hybrid functional accompanied by Lee−Yang−Parr correlation functional (B3LYP)[30] were employed in TD-DFT calculation without any symmetry constraints on molecular structures. The Hay and Wadt effective core potentials with a double-ζ basis set (LanL2DZ)[31] were applied for all atoms. Sixty singlet states (nstates = 60, singlet) are chosen in the calculations of the UV−vis absorption spectra and CD spectrum of complexes **1**−**4** and 80 singlet states (nstates = 80, singlet) for **5**. For computations of model Au_6 cluster, 40 singlet states (nstates = 40, singlet) are employed. The root is set as 1 in all of the TD-DFT calculations. Data for orbital composition analysis with Mulliken partition are from Gaussian 09 calculations and processed with Multiwfn software.[32] Plots of theoretical calculated CD spectra are conducted by using SpecDis software.[33]

DOI: 10.1021/jacs.6b01658
J. Am. Chem. Soc. 2016, 138, 5634−5643

■ ASSOCIATED CONTENT

Supporting Information

The Supporting Information is available free of charge on the ACS Publications website at DOI: 10.1021/jacs.6b01658.

Supporting figures, high-resolution ESI−MS, NMR spectra, experimental and calculated UV and CD spectra; HOMO to HOMO−3 and LUMO to LUMO+3 orbitals of **2**−**5**; orbital composition analysis with Mulliken partition of **1**−**5**; and input coordinates of model clusters at different dihedral angles (PDF)

X-ray data for compounds **1**-(***R,R***), **2**-(***R,R***), **3**-(***R,R***), **4**-(***rac***), and **5**-(***rac***) (CIF)

■ AUTHOR INFORMATION

Corresponding Author

*zhaolchem@mail.tsinghua.edu.cn

Notes

The authors declare no competing financial interest.

■ ACKNOWLEDGMENTS

Financial support by MOST (2013CB834501) and NNSFC (21132005, 21421064, 21522206) is gratefully acknowledged. This work is dedicated to Prof. Thomas C. W. Mak (Chinese University of Hong Kong) on the occasion of his 80th birthday. We are grateful to Prof. Mei-Xiang Wang (THU) for helpful discussions. Prof. De-Xian Wang (ICCAS) is acknowledged for the CD measurement.

■ REFERENCES

(1) Amabilino, D. B. *Chirality at the Nanoscale*; Wiley-VCH: Weinheim, 2009.

(2) Wang, Y.; Xu, J.; Wang, Y.; Chen, H. *Chem. Soc. Rev.* **2013**, *42*, 2930.

(3) (a) Knoppe, S.; Bürgi, T. *Acc. Chem. Res.* **2014**, *47*, 1318. (b) Ben-Moshe, A.; Maoz, B. M.; Govorov, A. O.; Markovich, G. *Chem. Soc. Rev.* **2013**, *42*, 7028. (c) Gautier, C.; Bürgi, T. *ChemPhysChem* **2009**, *10*, 483.

(4) (a) Yasukawa, T.; Miyamura, H.; Kobayashi, S. *Chem. Soc. Rev.* **2014**, *43*, 1450. (b) Gross, E.; Liu, J. H.; Alayoglu, S.; Marcus, M. A.; Fakra, S. C.; Toste, F. D.; Somorjai, G. A. *J. Am. Chem. Soc.* **2013**, *135*, 3881.

(5) (a) Shukla, N.; Bartel, M. A.; Gellman, A. J. *J. Am. Chem. Soc.* **2010**, *132*, 8575. (b) Xu, L.; Xu, Z.; Ma, W.; Liu, L.; Wang, L.; Kuang, H.; Xu, C. *J. Mater. Chem. B* **2013**, *1*, 4478. (c) Chen, Z.; Wang, Q.; Wu, X.; Li, Z.; Jiang, Y.-B. *Chem. Soc. Rev.* **2015**, *44*, 4249.

(6) (a) Baev, A.; Samoc, M.; Prasad, P. N.; Krykunov, M.; Autschbach, J. *Opt. Express* **2007**, *15*, 5730. (b) Fedotov, V. A.; Schwanecke, A. S.; Zheludev, N. I.; Khardikov, V. V.; Prosvirnin, S. L. *Nano Lett.* **2007**, *7*, 1996.

(7) (a) Valev, V. K.; Silhanek, A. V.; Verellen, N.; Gillijns, W.; Dorpe, P. V.; Aktsipetrov, O. A.; Vandenbosch, G. A. E.; Moshchalkov, V. V.; Verbiest, T. *Phys. Rev. Lett.* **2010**, *104*, 127401. (b) Knoppe, S.; Dass, A.; Bürgi, T. *Nanoscale* **2012**, *4*, 4211.

(8) Jadzinsky, P. D.; Calero, G.; Ackerson, C. J.; Bushnell, D. A.; Kornberg, R. D. *Science* **2007**, *318*, 430.

(9) Dolamic, I.; Knoppe, S.; Dass, A.; Bürgi, T. *Nat. Commun.* **2012**, *3*, 798.

(10) Lopez-Acevedo, O.; Tsunoyama, H.; Tsukuda, T.; Häkkinen, H.; Aikens, C. M. *J. Am. Chem. Soc.* **2010**, *132*, 8210.

(11) Wan, X.-K.; Yuan, S.-F.; Lin, Z.-W.; Wang, Q.-M. *Angew. Chem., Int. Ed.* **2014**, *53*, 2923.

(12) Schaaff, T. G.; Knight, G.; Shafigullin, M. N.; Borkman, R. F.; Whetten, R. L. *J. Phys. Chem. B* **1998**, *102*, 10643.

(13) Gautier, C.; Bürgi, T. *J. Am. Chem. Soc.* **2008**, *130*, 7077.

(14) Yanagimoto, Y.; Negishi, Y.; Fujihara, H.; Tsukuda, T. *J. Phys. Chem. B* **2006**, *110*, 11611.

(15) Pelayo, J. J.; Whetten, R. L.; Garzón, I. L. *J. Phys. Chem. C* **2015**, *119*, 28666.

(16) Noguez, C.; Garzón, I. L. *Chem. Soc. Rev.* **2009**, *38*, 757.

(17) (a) Qian, H.; Eckenhoff, W. T.; Zhu, Y.; Pintauer, T.; Jin, R. *J. Am. Chem. Soc.* **2010**, *132*, 8280. (b) Zeng, C.; Li, T.; Das, A.; Rosi, N. L.; Jin, R. *J. Am. Chem. Soc.* **2013**, *135*, 10011. (c) Crasto, D.; Malola, S.; Brosofsky, G.; Dass, A.; Häkkinen, H. *J. Am. Chem. Soc.* **2014**, *136*, 5000. (d) Chen, Y.; Zeng, C.; Liu, C.; Kirschbaum, K.; Gayathri, C.; Gil, R. R.; Rosi, N. L.; Jin, R. *J. Am. Chem. Soc.* **2015**, *137*, 10076. (e) Zeng, C.; Chen, Y.; Kirschbaum, K.; Appavoo, K.; Sfeir, M. Y.; Jin, R. *Sci. Adv.* **2015**, *1*, e1500045. (f) Zeng, C.; Chen, Y.; Liu, C.; Nobusada, K.; Rosi, N. L.; Jin, R. *Sci. Adv.* **2015**, *1*, e1500425. (g) Chen, J.; Zhang, Q.-F.; Williard, P. G.; Wang, L.-S. *Inorg. Chem.* **2014**, *53*, 3932.

(18) (a) Lechtken, A.; Schooss, D.; Stairs, J. R.; Blom, M. N.; Furche, F.; Morgner, N.; Kostko, O.; von Issendorff, B.; Kappes, M. M. *Angew. Chem., Int. Ed.* **2007**, *46*, 2944. (b) Karttunen, A. J.; Linnolahti, M.; Pakkanena, T. A.; Pyykkö, P. *Chem. Commun.* **2008**, 465. (c) Malola, S.; Lehtovaara, L.; Knoppe, S.; Hu, K.-J.; Palmer, R. E.; Bürgi, T.; Häkkinen, H. *J. Am. Chem. Soc.* **2012**, *134*, 19560. (d) Pei, Y.; Lin, S.; Su, J.; Liu, C. *J. Am. Chem. Soc.* **2013**, *135*, 19060.

(19) Nesmeyanov, A. N.; Perevalova, E. G.; Struchkov, Y. T.; Antipin, M. Y.; Grandberg, K. I.; Dyadchenko, V. P. *J. Organomet. Chem.* **1980**, *201*, 343.

(20) (a) Ramamoorthy, V.; Sharp, P. R. *Inorg. Chem.* **1990**, *29*, 3336. (b) Grohmann, A.; Riede, J.; Schmidbaur, H. *J. Chem. Soc., Dalton Trans.* **1991**, 783. (c) López-de-Luzuriaga, J. M.; Sladek, A.; Schier, A.; Schmidbaur, H. *Inorg. Chem.* **1997**, *36*, 966. (d) Shan, H.; Yang, Y.; James, A. J.; Sharp, P. R. *Science* **1997**, *275*, 1460.

(21) (a) Pyykkö, P. *Chem. Rev.* **1997**, *97*, 597. (b) Schmidbaur, H.; Schier, A. *Chem. Soc. Rev.* **2008**, *37*, 1931. (c) Schmidbaur, H.; Schier, A. *Chem. Soc. Rev.* **2012**, *41*, 370.

(22) (a) Kobayashi, R.; Nonoguchi, Y.; Sasaki, A.; Yao, H. *J. Phys. Chem. C* **2014**, *118*, 15506. (b) Barcaro, G.; Sementa, L.; Fortunelli, A.; Stener, M. *Phys. Chem. Chem. Phys.* **2015**, *17*, 27952.

(23) Wang, Q.-M.; Lee, Y.-A.; Crespo, O.; Deaton, J.; Tang, C.; Gysling, H. J.; Gimeno, M. C.; Larraz, C.; Villacampa, M. D.; Laguna, A.; Eisenberg, R. *J. Am. Chem. Soc.* **2004**, *126*, 9488.

(24) Dolamic, I.; Varnholt, B.; Bürgi, T. *Nat. Commun.* **2015**, *6*, 7117.

(25) Zhu, M.; Qian, H.; Meng, X.; Jin, S.; Wu, Z.; Jin, R. *Nano Lett.* **2011**, *11*, 3963.

(26) Fan, Z.; Govorov, A. O. *Nano Lett.* **2012**, *12*, 3283.

(27) Provorse, M. R.; Aikens, C. M. *J. Am. Chem. Soc.* **2010**, *132*, 1302.

(28) Sheldrick, G. M. *Acta Crystallogr., Sect. A: Found. Crystallogr.* **2008**, *A64*, 112.

(29) Frisch, M. J.; Trucks, G. W.; Schlegel, H. B.; Scuseria, G. E.; Robb, M. A.; Cheeseman, J. R.; Scalmani, G.; Barone, V.; Mennucci, B.; Petersson, G. A.; Nakatsuji, H.; Caricato, M.; Li, X.; Hratchian, H. P.; Izmaylov, A. F.; Bloino, J.; Zheng, G.; Sonnenberg, J. L.; Hada, M.; Ehara, M.; Toyota, K.; Fukuda, R.; Hasegawa, J.; Ishida, M.; Nakajima, T.; Honda, Y.; Kitao, O.; Nakai, H.; Vreven, T.; Montgomery, J. A.; Peralta, J. E.; Ogliaro, F.; Bearpark, M.; Heyd, J. J.; Brothers, E.; Kudin, K. N.; Staroverov, V. N.; Kobayashi, R.; Normand, J.; Raghavachari, K.; Rendell, A.; Burant, J. C.; Iyengar, S. S.; Tomasi, J.; Cossi, M.; Rega, N.; Millam, J. M.; Klene, M.; Knox, J. E.; Cross, J. B.; Bakken, V.; Adamo, C.; Jaramillo, J.; Gomperts, R.; Stratmann, R. E.; Yazyev, O.; Austin, A. J.; Cammi, R.; Pomelli, C.; Ochterski, J. W.; Martin, R. L.; Morokuma, K.; Zakrzewski, V. G.; Voth, G. A.; Salvador, P.; Dannenberg, J. J.; Dapprich, S.; Daniels, A. D.; Farkas, O.; Foresman, J. B.; Ortiz, J. V.; Cioslowski, J.; Fox, D. J. *Gaussian 09*, revision A.02; Gaussian, Inc.: Wallingford, CT, 2009.

(30) (a) Becke, A. D. *J. Chem. Phys.* **1993**, *98*, 5648. (b) Lee, C.; Yang, W.; Parr, R. G. *Phys. Rev. B: Condens. Matter Mater. Phys.* **1988**, *37*, 785.

(31) (a) Wadt, W. R.; Hay, P. J. *J. Chem. Phys.* **1985**, *82*, 284. (b) Hay, P. J.; Wadt, W. R. *J. Chem. Phys.* **1985**, *82*, 270. (c) Hay, P. J.;

DOI: 10.1021/jacs.6b01658
J. Am. Chem. Soc. 2016, 138, 5634−5643

Wadt, W. R. *J. Chem. Phys.* **1985**, *82*, 299. (d) Dunning, T. H., Jr.; Hay, P. J. In *Methods of Electronic Structure, Theory*; Schaefer, H. F., III, Ed.; Plenum Press: New York, 1977; Vol. 2.
(32) Lu, T.; Chen, F. *J. Comput. Chem.* **2012**, *33*, 580.
(33) Bruhn, T.; Schaumlöffel, A.; Hemberger, Y. *SpecDis 1.63*; University of Wuerzburg: Germany, 2015.

DOI: 10.1021/jacs.6b01658
J. Am. Chem. Soc. 2016, 138, 5634−5643